



ELSEVIER

Available online at www.sciencedirect.com

SCIENCE @ DIRECT®

Nuclear Instruments and Methods in Physics Research A 506 (2003) 304–315

**NUCLEAR
INSTRUMENTS
& METHODS
IN PHYSICS
RESEARCH**
Section Awww.elsevier.com/locate/nima

Z-dependent spectral measurements of SASE FEL radiation at APS[☆]

V. Sajaev*, Z. Huang, S.G. Biedron, P.K. Den Hartog, E. Gluskin, K.-J. Kim, J.W. Lewellen, Y. Li, O. Makarov, S.V. Milton, E.R. Moog

Advanced Photon Source, Argonne National Laboratory, Argonne, IL 60439, USA

Abstract

We report on the first measurements of the dependence on the axial distance z of the spectrum of self-amplified spontaneous emission free-electron laser (SASE FEL) radiation. The measurements are performed under different FEL conditions in the wavelength range from 265 to 530 nm. Spectral measurements of the radiation at FEL saturation are included. The z -dependence of the radiation spectrum is compared with theory and simulations.

© 2002 Elsevier Science B.V. All rights reserved.

PACS: 41.60.Cr

Keywords: Free-electron laser; Spectrum; Self-amplified spontaneous emission

1. Introduction

The low-energy undulator test line (LEUTL) at the Advanced Photon Source (APS) was designed to conduct experiments on the self-amplified spontaneous emission free-electron laser (SASE FEL) process in the visible and ultraviolet wavelengths. It was built as an extension of the existing APS linac and includes a photocathode rf gun, a linear accelerator with a bunch compressor, an electron beam transport line, and an undulator system.

The photocathode rf gun generates high-current low-emittance electron bunches at 6 Hz. The linear accelerator can accelerate the electron beam up to a maximum of 650 MeV, but for present SASE experiments the energy ranges from 217 MeV to 300 MeV. The undulator system consists of nine identical 2.4 m long undulators separated from each other by a 38 cm drift space containing a visible light diagnostics (VLD) station, and quadrupole and corrector magnets. The undulator period is 3.3 cm, the peak field is 1 T, and the undulator parameter K is 3.1. A detailed description of the LEUTL and its various component systems can be found in Refs. [1–4].

In 2001, outstanding results were obtained at the LEUTL; the gain from the first undulator to the saturation point of the order of 10^6 was measured, and the saturation of the SASE FEL process was achieved in visible and ultraviolet [5].

[☆]Work supported by the US Department of Energy, Office of Basic Energy Sciences, under Contract No. W-31-109-ENG-38. This paper was presented at the 23rd Free Electron Laser Conference, Darmstadt, Germany, August 20–24, 2001.

*Corresponding author.

E-mail address: sajaev@aps.anl.gov (V. Sajaev).

In this paper we present and discuss spectral data of the SASE light gathered during that time, comparing the data with theory and simulation results. The paper begins with the description of a high-resolution spectrometer. Then it describes the spectrum measurements and presents the dependence on z , the axial distance along the undulator, of the spectral measurements of the SASE light. Simulation results are also presented to compare with the measurements. Finally, the dependence of the radiated wavelength on the vertical angle is discussed, and an example of the second harmonic spectrum is demonstrated.

2. Spectrometer description

All spectral measurements reported in this paper have been obtained with a high-resolution spectrometer located at the downstream end of the undulator line in the end-station room. A mirror at each diagnostic station can direct the SASE light towards the spectrometer through a hole in the shielding wall, thus allowing the measurement

of the spectral characteristics of the SASE light at different longitudinal locations along the undulator.

A schematic of the spectrometer is shown in Fig 1. It utilizes a Paschen–Runge mount which provides independence on the angle of the incoming light, and tunability over a wide range of wavelengths. The spectrometer consists of three main elements on the Rowland circle: a vertical entrance slit, a spherical grating, and a CCD camera. The light coming from the undulator hall is focused on the entrance slit with a concave mirror. All optical elements are reflective with metal coatings, allowing the system to operate over a wide range of wavelengths. The CCD camera can measure the radiation of each electron bunch separately. To reduce the dark current and to improve the signal-to-noise ratio, the CCD camera is cooled.

The spectrometer was calibrated with hollow cathode discharge lamps, and the designed resolution was checked on different wavelengths. The main parameters of the spectrometer are presented in Table 1.

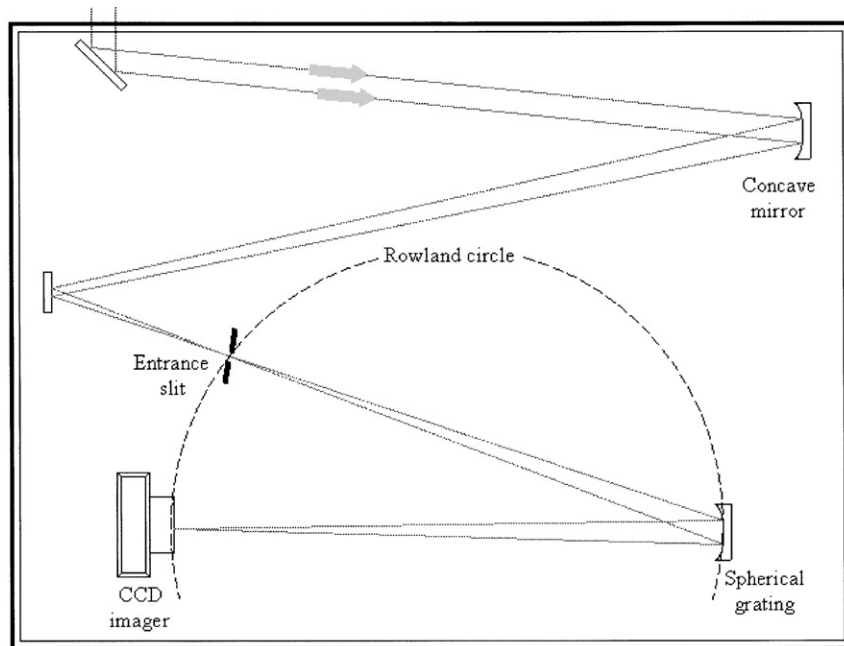


Fig. 1. A top view of the Paschen–Runge-type spectrometer for the analysis of the SASE FEL light.

3. Spectrum measurements

A typical spectrum of the spontaneous undulator radiation measured after the second section of the undulator is shown in Fig. 2. In order to explain the spectrum, let us consider the microscopic picture of the electron beam current at the entrance into the undulator; it is a sum of the contributions by electrons, the k -th electron arrives at the entrance of the undulator at time t_k :

$$I(t) = -e \sum_{k=1}^N \delta(t - t_k) \quad (1)$$

where N is the number of electrons in a bunch. The Fourier transform of the current can be

Table 1
Main parameters of the high-resolution Paschen–Runge spectrometer

Grating	
Grooves/mm	600
Curvature radius (mm)	1000
Blaze wavelength (nm)	482
CCD camera	
Number of pixels	1100 × 330
Pixel size (μm)	24
Concave mirror curvature radius (mm)	4000
Spectral resolution (Å)	0.4
Bandpass (nm)	44
Resolving power at 530 nm	10 000
Wavelength range (nm)	250–1100

written as

$$\bar{I}(\omega) = \int_{-\infty}^{\infty} e^{i\omega t} I(t) dt = -e \sum_{k=1}^N e^{i\omega t_k} \quad (2)$$

and the Fourier transform of the electric field emitted in the undulator can be expressed by

$$E(\omega) = e(\omega) \sum_k e^{i\omega t_k} \quad (3)$$

where $e(\omega)$ is the Fourier transform of an individual particle traveling through the undulator and is proportional to $\sin(\omega - \omega_0)T/(\omega - \omega_0)T$. The summation of a large number of exponentials with different arguments results in an appearance of sharp spikes in the $E(\omega)$ dependence, as seen in Fig. 2. The spectrum consists of typical spikes, the width of which is approximately the reciprocal of the electron bunch length [6,7].

The typical single shot spectra of the SASE light measured at different locations along the undulator line are presented in Fig. 3 (left column). The typical spectra simulated with the FEL code GINGER [8] for the same locations are shown in the right column.

3.1. Spectrum bandwidth

From the 1D theory of SASE, we know that in the exponential gain regime the spectrum width of

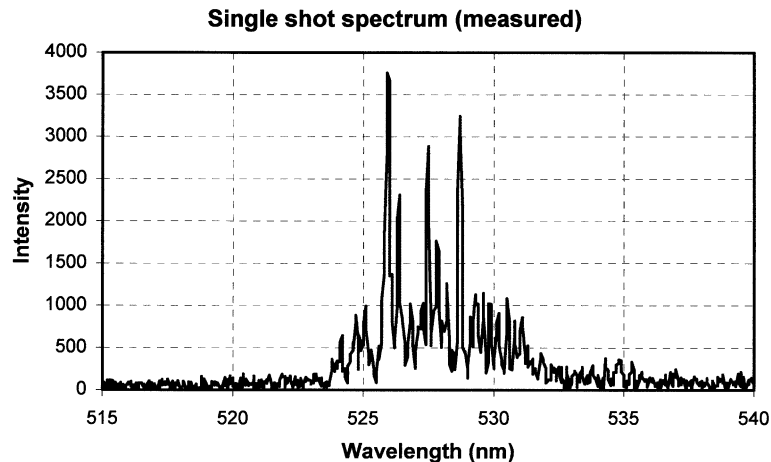


Fig. 2. Measured spectrum of spontaneous undulator radiation. FWHM bunch length is about 4 ps.

Single shot spectra

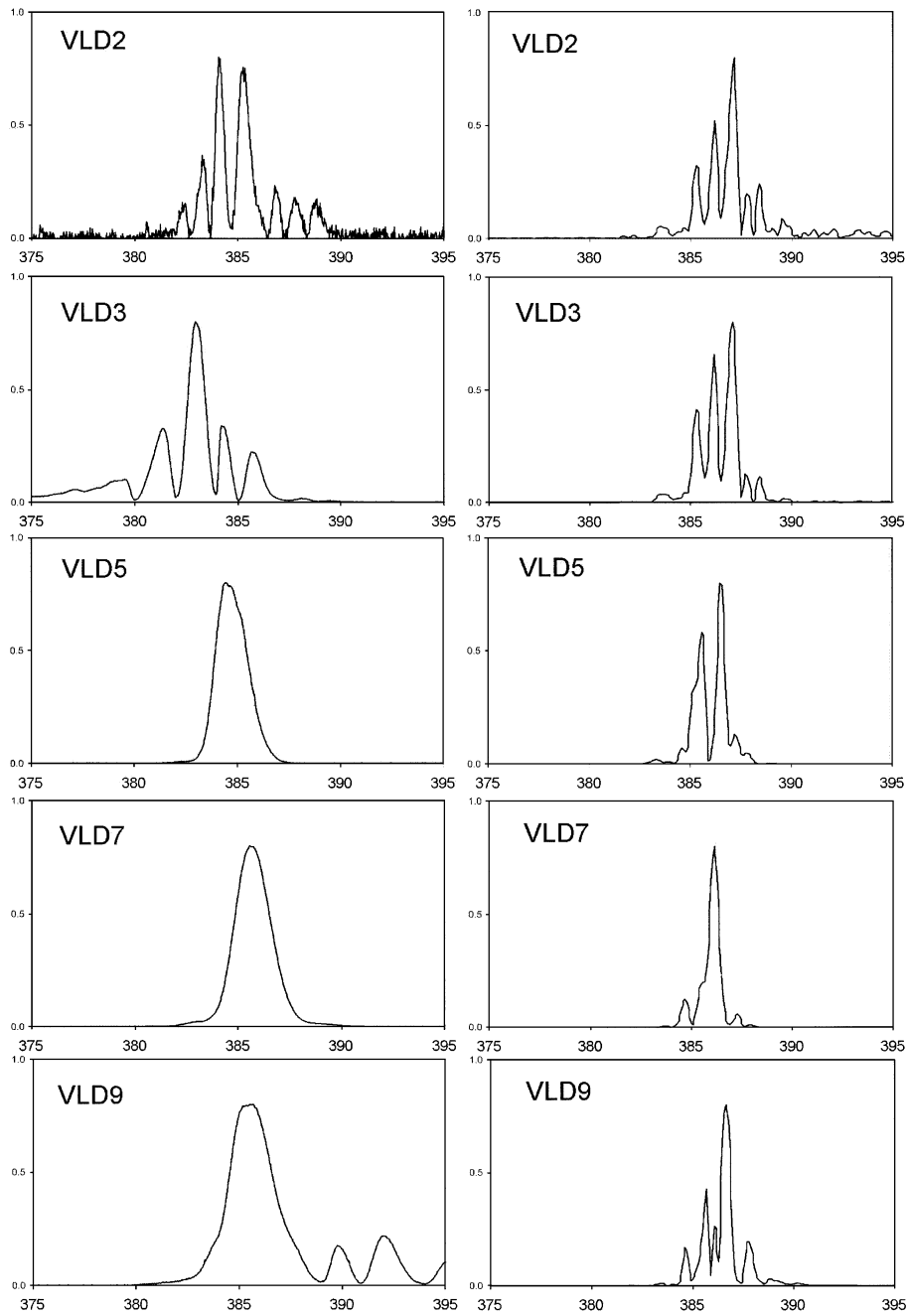


Fig. 3. Z-dependent single-shot spectrum measurements of the SASE radiation (left column) and simulations (right column). The saturation is achieved around undulator 7 (VLD 7).

the SASE light is given by [9]

$$\frac{\delta\lambda}{\lambda} = \sqrt{\frac{0.83\rho}{N_U}} \sim \frac{1}{\sqrt{z}} \quad (4)$$

where N_U is the number of undulator periods, ρ is the FEL scaling parameter, and z is the distance along the undulator.

Fig. 4 demonstrates the z -dependent rms spectrum width for both measurements and simulations (the simulations were done with the beam parameters shown in Ref. [5], Table 1, case C). The spectrum width indeed decreases along the undulator in agreement with Eq. (4), until saturation is reached at undulator number 7. After saturation, the spectrum width increases again due to the synchrotron instability of the electrons and side-band development.

The measured and simulated curves of Fig. 4 show very similar z -dependent behavior. However, the absolute value of the measured spectrum width is about a factor of 1.6 larger than that obtained by simulations. The reason for the difference is not understood.

3.2. Spike width

For spontaneous radiation the width of the spectral spikes is given by the reciprocal of the bunch length. However, we expect this behavior to be modified in the case of SASE because radiation emitted by different parts of the beam experiences different gain. One can view it as a decrease in the effective bunch length, since the radiation intensity in the central part of the Gaussian beam grows faster than in the rest of the beam. Therefore, the spike width will increase during the exponential gain regime. At saturation, other parts of the beam with lower local beam current will also come to saturation. This will result in an increase in the effective bunch length and a decrease in the spike width.

The spike width can be extracted from an autocorrelation of the spectrum. Fig. 5 shows the autocorrelation averaged over many shots for several VLD stations for simulated and measured spectra. The z -dependence of the spike width obtained with the autocorrelation is plotted in Fig. 6. As expected, the spike width increases in the exponential gain regime up to saturation, and then it decreases as expected. The measured and

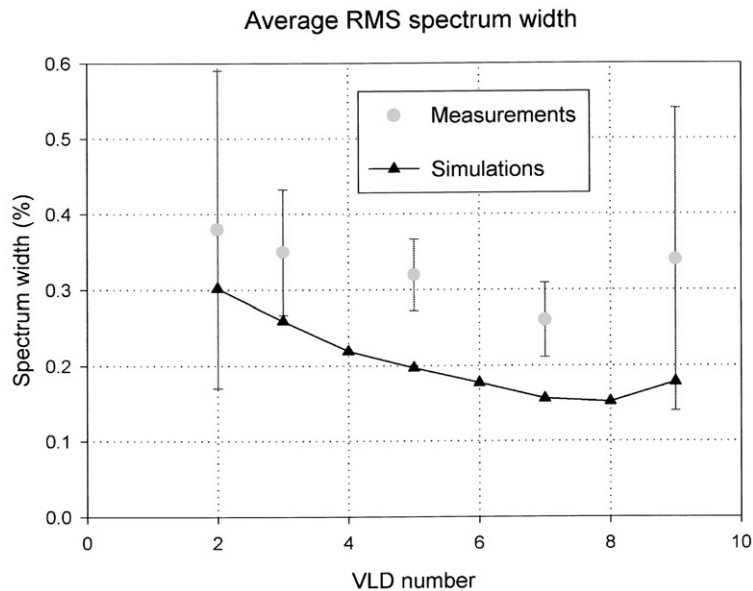


Fig. 4. RMS spectrum width for measurements and simulations. Error bars show standard deviation of the width fluctuations.

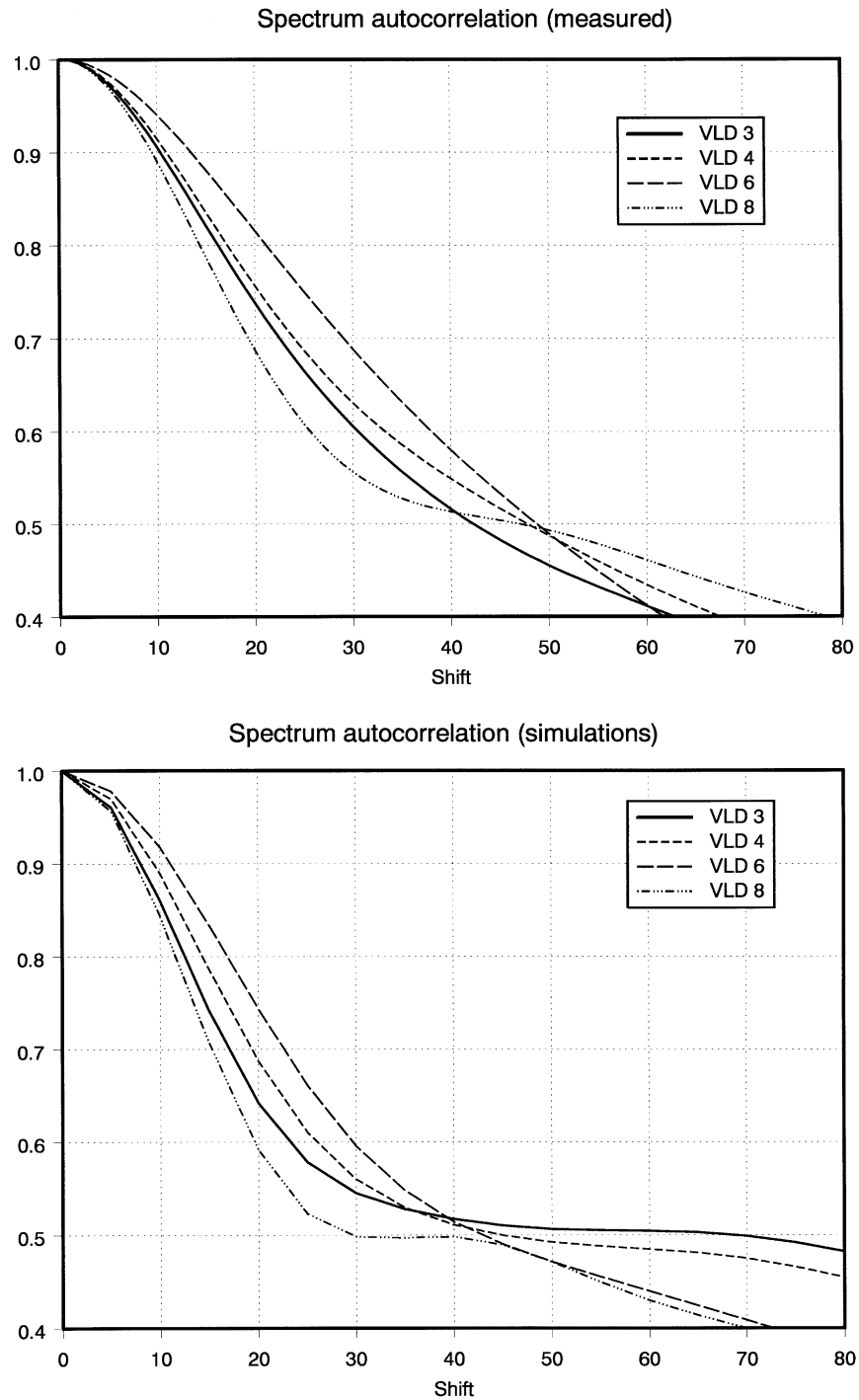


Fig. 5. Average spectrum autocorrelation for measured (top) and simulated (bottom) spectra.

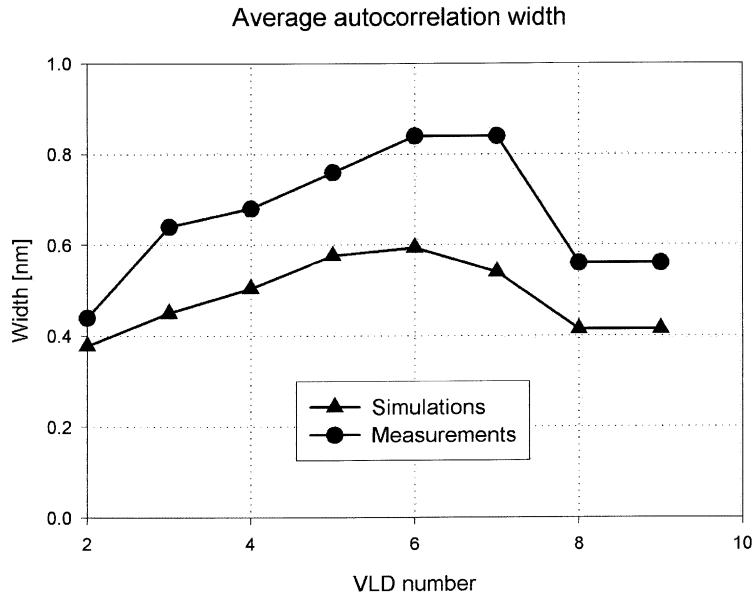


Fig. 6. Average spike width along the undulator line for measured and simulated spectra.

calculated spike widths of Fig. 6 show similar behavior along the undulator line; however, the absolute spike width of the measured spectra is again about a factor of 1.5 larger, similar to the case of the spectrum width in Fig. 3.

The discrepancy in the computed and measured spike widths can be explained as follows: the estimated accuracy of the electron bunch length measurements is about 20% rms. This could give an error close to a factor of 1.5. Furthermore, the bunch profile could contain an intense core that is shorter than the overall bunch but provides most of the radiation.

3.3. Average number of spikes

As one can see from Fig. 3, the number of spikes in the spectrum also decreases with the distance along the undulator. The number of spectral spikes is roughly the number of coherence modes. Since the coherence length increases along the undulator, the number of coherent modes decreases, resulting in a decreased number of spikes. When saturation is achieved, the sidebands appear, increasing the number of spikes again as one

can see from the last row in Fig. 3. An average number of spikes in the spectrum calculated for different locations along the undulator line is presented in Fig. 7.

4. Vertical angle dependence of the wavelength

Due to astigmatism of the spherical grating in the spectrometer, the horizontal and vertical focuses of the spectral image are not achieved simultaneously. Thus the image on the CCD camera has non-zero vertical size due to the vertical angle spread in the SASE light.

Fig. 8 shows one of the images recorded by the CCD camera. The horizontal axis of the image represents the wavelength of the radiation while the vertical axis represents the vertical angle of the radiation. Analysis of such images allows one to extract the dependence of the radiated wavelength of the SASE light on vertical angle.

During the exponential growth of SASE light, a single transverse mode dominates over all other modes at a given radiation wavelength within the gain bandwidth. However, the mode

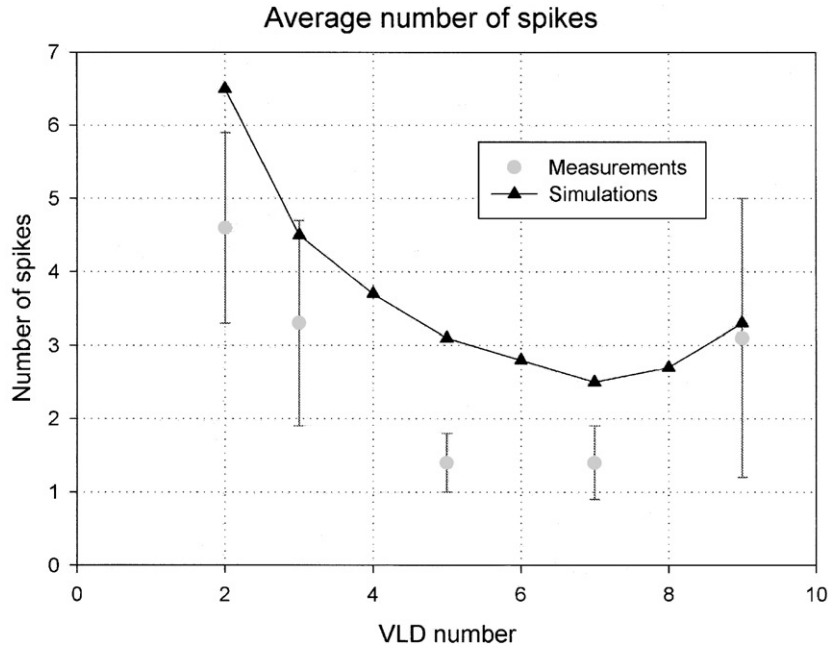


Fig. 7. Average number of spikes in the spectrum at different locations along the undulator. Error bars show standard deviation of the number of spike fluctuations.

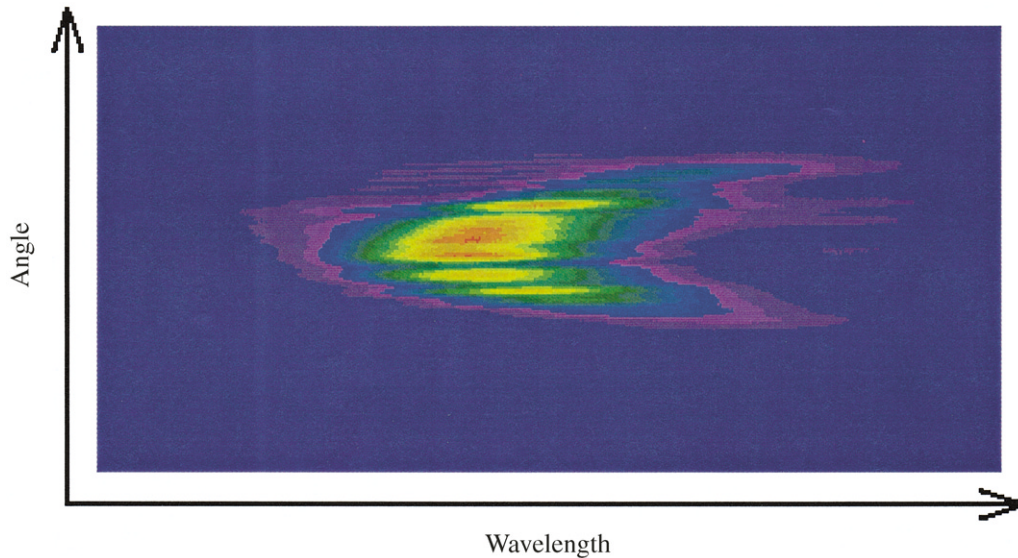


Fig. 8. Spectral image of the radiation after VLD 4. Horizontal direction is wavelength; vertical direction is vertical angle of radiation.

characteristics at one wavelength are different from that at another wavelength [10]. Specifically, the angular divergence of the transverse mode increases somewhat with the increasing wavelength

due to stronger diffraction. As a result, the central wavelength observed at an angle θ with respect to the z -axis is slightly red-shifted. Fig. 9 shows the measured central wavelength as a function of the

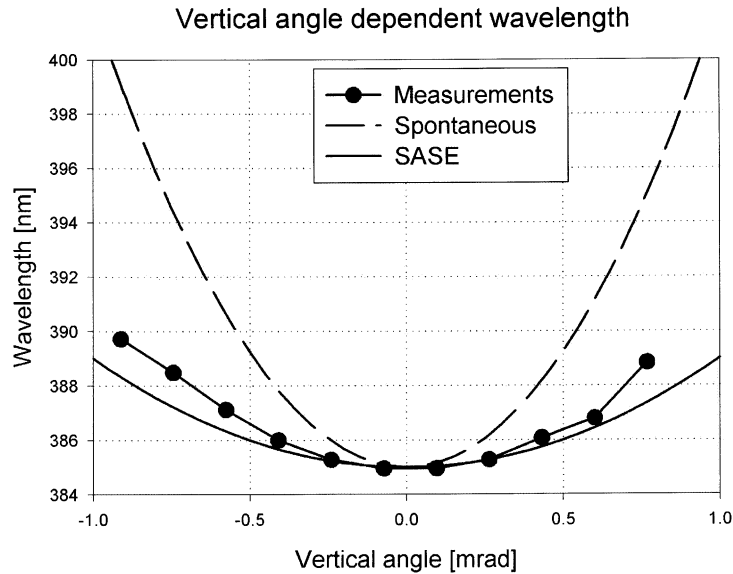


Fig. 9. Wavelength dependence on the vertical radiation angle. Dash and solid lines are expected curve for the spontaneous emission and for SASE radiation; circles are measurements.

vertical angle, obtained from the image shown above. Calculations based on the 3D FEL mode theory show close agreement (solid curve). For comparison, the angular dependence of the radiation wavelength for spontaneous emission is also shown (dashed curve), which is given by

$$\frac{\delta\lambda}{\lambda} = \frac{\gamma^2\theta^2}{1 + K^2/2}$$

where γ is the relativistic factor of the electron beam and K is the undulator parameter. As expected, the angular dependence is much stronger for spontaneous emission than for SASE.

We should remark that the measured spectrum width and spike width can be increased due to the curvature of the spectral image. The image processing software extracts a curve by integrating over some vertical intervals of the image, so the resulting spectrum can be wider than the original one. Accurate comparisons of spectral images with their integrated projections show that a spectrum width increase of up to 20% is possible, when the vertical integration intervals are not optimally chosen.

The spectral images can also be used for determining the angular distribution of the radiation

intensity. Fig. 10 shows the intensity plot obtained from the image above. This plot gives rms angular divergence of the SASE radiation of 0.5 mrad, which is in good agreement with the values obtained from other measurements.

5. Second harmonic measurements

The non-linear harmonics of the fundamental wavelength are expected to grow after the bunching at the fundamental is developed [11,12]. In the case of a planar undulator, the odd harmonics are favored due to the natural sinusoidal motion of the electron beam in the undulator, although the second harmonics could be fairly substantial. From the simulations [11], one can expect second harmonic power at about 10^{-3} of the fundamental.

Minor modification of the spectrometer configuration allows measurement of the spectrum of the first and second harmonics of the SASE radiation simultaneously. The CCD camera is placed at the location of the spectral image of the second harmonic, and one additional mirror at the center of the Rowland circle is used to direct the image of the first harmonic onto the CCD. Fig. 11 shows a

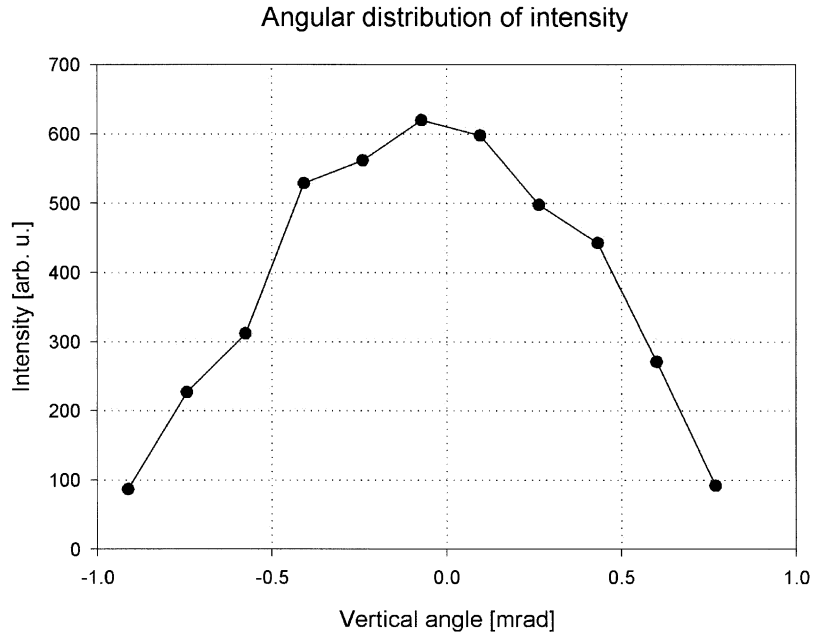


Fig. 10. Angular distribution of the SASE radiation intensity.

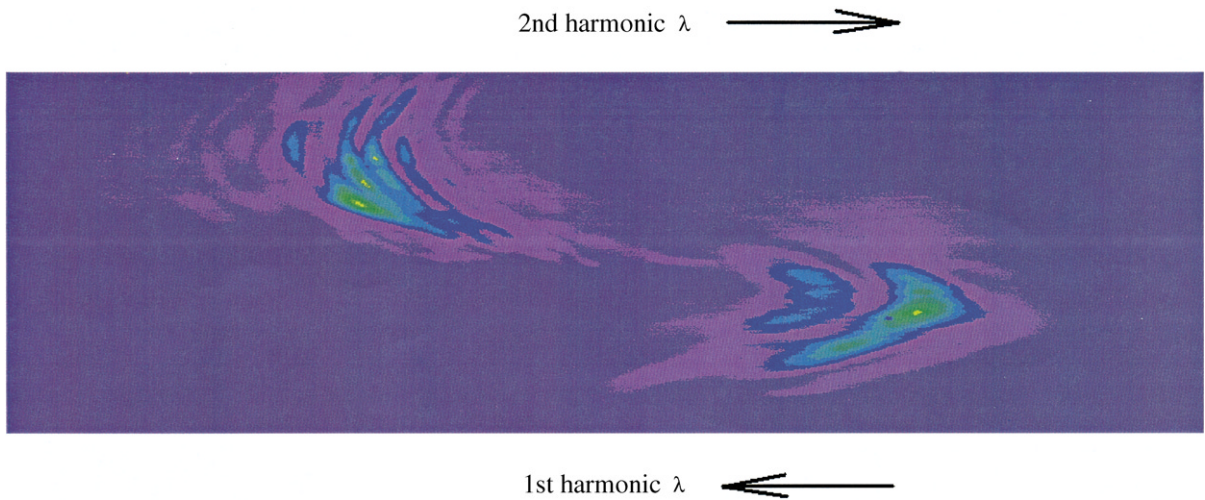


Fig. 11. Spectral image showing simultaneously first and second harmonics of the SASE radiation. Top left part of the image is the second harmonic spectrum; bottom right is the first harmonic spectrum. Wavelength direction is reversed for the first harmonic image because one more mirror was used to direct the first harmonic image onto the CCD camera.

typical spectral image with two spectra: the upper one is the second harmonic spectrum and the lower one is the fundamental harmonic. The first harmonic was attenuated by a factor of 10^3 .

Fig. 12 shows two typical plots showing the first and second harmonic spectra. These two plots were chosen to demonstrate that the spectral shape of the two harmonics could be different (left) or similar (right). The average rms spectrum width of

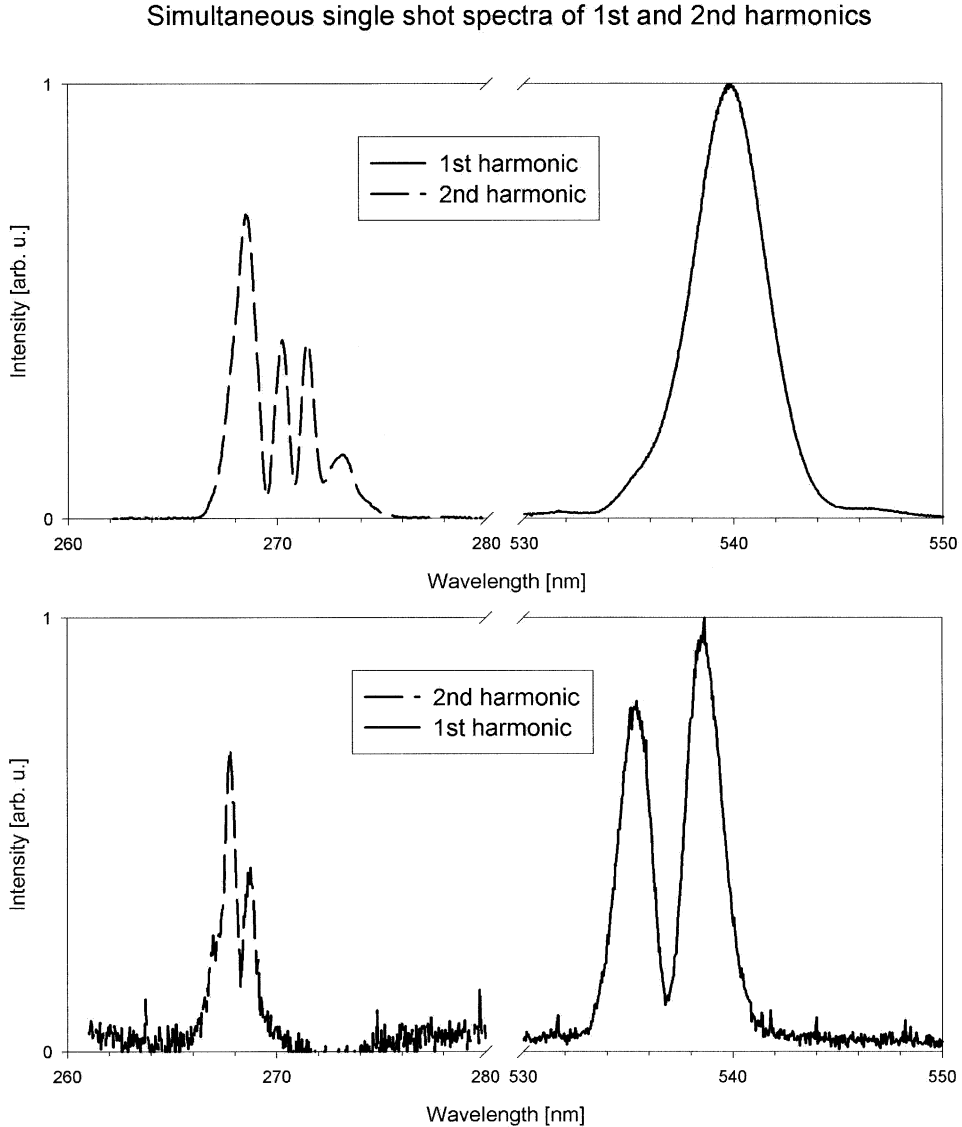


Fig. 12. Spectral plots showing simultaneous measurements of the first (solid curve) and second (dashed curve) harmonics for two different shots.

the two harmonics has been calculated for the SASE radiation after the undulator 7

$$\text{1st harmonic (530 nm)} \quad \frac{\delta\lambda}{\lambda} = 2.9 \times 10^{-3}$$

$$\text{2nd harmonic (265 nm)} \quad \frac{\delta\lambda}{\lambda} = 4.4 \times 10^{-3}.$$

6. Conclusions

The z -dependence of the spectrum of SASE FEL radiation has been measured. Qualitative behavior of the measured spectra coincides very well with the theory and simulations exhibiting a narrowing of the spectral bandwidth during the exponential gain regime and the appearance of sidebands after

saturation is achieved. However, there are still some quantitative differences that could be attributed to both measurement processing difficulties and simulation complexity. It is hoped that these data will further stimulate SASE modeling development for the fundamental and higher harmonics.

References

- [1] S.V. Milton, et al., Nucl. Instr. and Meth. A 407 (1998) 210.
- [2] S.V. Milton, et al., Proc. SPIE 3614 (1999) 96.
- [3] I.B. Vasserman, et al., Proceedings of the PAC 1999, p. 2489.
- [4] E. Gluskin, et al., Nucl. Instr. and Meth. A 429 (1999) 358.
- [5] S. Milton, et al., Science 292 (2001) 2037. Originally published in Science Express as 10.1126/science.1059955 on May 17, 2001.
- [6] M. Zolotarev, G. Stupakov, SLAC-PUB-7132, March 1996.
- [7] E. Saldin, E. Schneidmiller, M. Yurkov, Statistical properties of radiation from VUV and X-ray FEL, DESY preprint TESLA-FEL97-02, April 1997.
- [8] W. Fawley, An informal manual for GINGER and its post-processor XPLOTGIN, BP Technical Note-104, LBNL, Berkeley, CA, 1995.
- [9] K.-J. Kim, Nucl. Instr. and Meth. A 250 (1986) 396.
- [10] K.-J. Kim, Z. Huang, Present Status of X-ray FELs, AIP Conference Proceedings 581, Physics of and Science with the X-ray Free-Electron Laser, 2001, p. 185.
- [11] H.P. Freund, S.G. Biedron, S.V. Milton, IEEE J. Quant. Electron. 36 (2000) 275 and references therein.
- [12] Z. Huang, K.-J. Kim, Phys. Rev. 62E (2000) 7295 and references therein.